Scalable pillar[5]arene-integrated poly(arylate-amide) molecular sieve membranes to separate light gases

Woochul Song[a†#], Jaesung Park[ab†], Subhadeep Dasgupta[c], Chenhao Yao[a], Nikhil Maroli[c], Harekrushna Behera[d], Xinyang Yin[e], Durga P. Acharya[f], Xueyi Zhang[e], Cara M. Doherty[f], Prabal K. Maiti[c], Benny D. Freeman[a*] and Manish Kumar[ad*]

[a]McKetta Department of Chemical Engineering, The University of Texas at Austin, Austin, TX 78712, USA
[b]Green Carbon Research Center, Korea Research Institute of Chemical Technology (KRICT), Gajeong-ro 141, Yuseong-gu, Daejeon, 34114, Republic of Korea
[c]Center for Condensed Matter Theory, Indian Institute of Science, Bangalore 560012, India
[d]Department of Civil, Architectural and Environmental Engineering, The University of Texas at Austin, Austin, TX 78712, USA
[e]Department of Chemical Engineering, The Pennsylvania State University, University Park, PA 16802, USA
[f]CSIRO Manufacturing Flagship, Private Bag 10, Clayton South, Victoria 3169, Australia

[*]Email (M.K.): manish.kumar@utexas.edu
[*]Email (B.D.F.): freeman@che.utexas.edu

[†]W.S. and J.P. contributed equally to this paper.

Abstract

Molecular sieve membranes and their analogs could potentially transform energy intensive gas separation processes. However, many such membranes suffer from either limited processability or physical stability including plasticization of semi-flexible microstructures. Here, we report on a new variation of all-polymer-based molecular sieve membranes that could tackle these specific challenges. These membranes were prepared by interfacial polymerization of pillar[5]arene, *m*-phenylenediamine, and trimesoyl chloride to create characteristic poly(arylate-amide) heteropolymer microstructures. Pillar[5]arenes were crosslinked into the films with net weight fractions of up to ~47 %, wherein the 4.7 Å cavities of pillar[5]arenes were interconnected with ~2.8 Å apertures. These microstructures provided preferred permeation paths for smaller molecules (He and H_2) among the tested light gases (He, H_2, CO_2, O_2, N_2, and CH_4), and resulted in significant molecular sieving effects with representative pure gas selectivities of 32 (H_2/CO_2), 150 (CO_2/CH_4), 4600 (H_2/CH_4), 13 (O_2/N_2), and 4.7 (N_2/CH_4) at 35 °C and 10 atm. These separation factors outperform most polymer-based gas separation membranes, while providing membrane features such as thin film barriers, cross-linked polymer backbones, and excellent processability resulting from interfacial polymerization that are critical for large scale operations.

1. Introduction

Membrane gas separations are an attractive technology for mitigating increasing global energy demands for chemical separations.[1, 2] Specifically, molecular sieve membranes such as inorganic microporous or carbon molecular sieve (CMS) membranes present great potential for redesigning energy intensive gas separation processes.[3] However, wide adaptation of membranes in these applications has been challenging with current membrane formats, where strong molecular sieving effects are necessary to, for example, separate nitrogen from natural gas. This is because most membranes have rather poor selectivity for N_2/CH_4 separation, and because of practical challenges faced when membranes are considered for applications, such as cost, large-scale processibility, and physical and chemical stability.[4] To tackle these challenges, it is important to develop new membranes that possess (1) covalently secured and controlled microstructures to achieve both good molecular sieving properties and physical stability,[3] and (2) capability for large scale processing membranes with thin barrier layers.[5]

Thin-film composite (TFC) membranes prepared by interfacial polymerization (IP) could be a promising

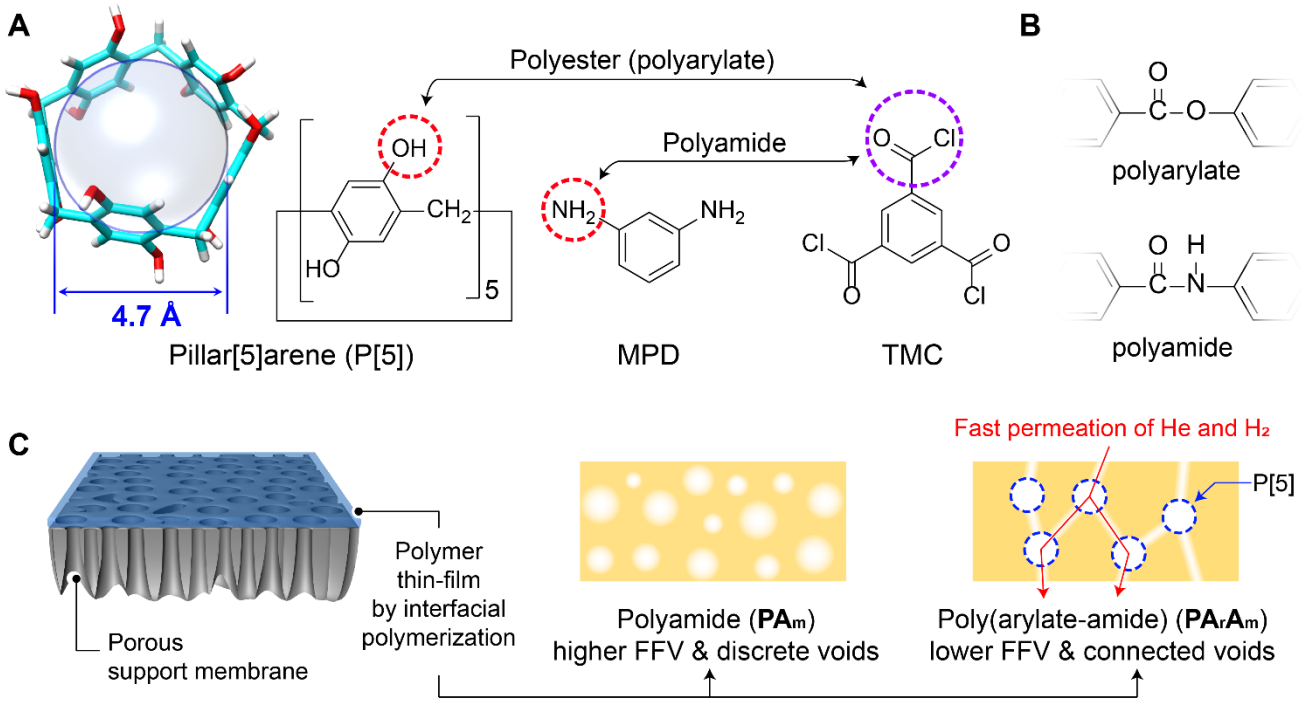

Figure 1. Polyamide (PA_m) and polyarylate-polyamide (PA_rA_m) thin film composite (TFC) membranes prepared by interfacial polymerization. (A) Chemical structures of P[5], MPD, and TMC monomers. (B) Chemical structures of PA_r and PA_m backbones formed by interfacial polymerization reactions. (C) Schematic illustration of the TFC membranes with PA_m and PA_rA_m polymer films. Schematics in this panel are not scaled with molecular details but presented to provide conceptual structure-to-transport relationship of PArAm membranes.

membrane platform in this regard. IP uses polycondensation reactions to create highly cross-linked polyamide polymer films. This chemistry enables formation of sub-micron thin selective layers, secure good mechanical stability through high degree of cross-linking, and are already used to produce industrial scale membranes via continuous roll-to-roll processes. Those practical features make TFC membranes widely adopted in water-related large-scale processes such as desalination, and wastewater recycling. It also makes current TFC membrane market valued at $7 billion (USD) which is projected to reach $13.5 billion by 2025.[6] However, TFC membranes have not been very successful in gas separations due to the challenges of both avoiding defect formation and tuning the microstructures at the sub-angstrom scale.

Here, we present pillar[5]arene-integrated TFC membranes to help address these challenges. These membranes were prepared by interfacial polymerization of pillar[5]arene (P[5]), *m*-phenylenediamine (MPD), and trimesoyl chloride (TMC) monomers, where P[5] and MPD react with TMC to form cross-linked polyarylate (PAr) and polyamide (PAm) polymer backbones, respectively (**Figure 1A** and **1B**). As a result, the P[5]s are covalently integrated into the thin poly(arylate-amide) (PArAm) selective layers with up to ~47 % (w/w), leading to interconnection of 4.7 Å cavities of P[5]s with 2.8 Å micro-apertures (**Figure 1C**). Such a unique free volume network provides interconnected permeation paths for He and H_2 and maximized molecular sieving ability for light gases such as CO_2, O_2, N_2, and CH_4.

2. Results and Discussion

P[5]-integrated PArAm TFC membranes were prepared using conventional interfacial polymerization (IP) method.[7] The concept of using macrocyclic molecules to make PAr or PAm TFC membranes by IP reactions were previously reported[8-10] but, to the best of our knowledge, no gas separation results has been reported, presumably due to the challenge of defect formation during membrane fabrication. In this study, by introducing polyamide chemistry via conventional MPD monomers to make heteropolymer structures, defect-free PArAm thin films could be readily prepared, and they were stable at gas permeation pressures higher than 30 atm. Briefly, the base-activated phenoxide form of P[5] and MPD were dissolved in water, and TMC was dissolved in anhydrous *n*-hexane at different concentrations for IP reactions. Polyethersulfone (PES) membranes were used as support membranes, and the reaction time was 10 minutes unless otherwise specified. Conventional PAm TFC membranes were also prepared as a comparison by just using MPD and TMC monomers without P[5]. More details including monomer concentrations and membrane fabrication processes can be found in the experimental section.

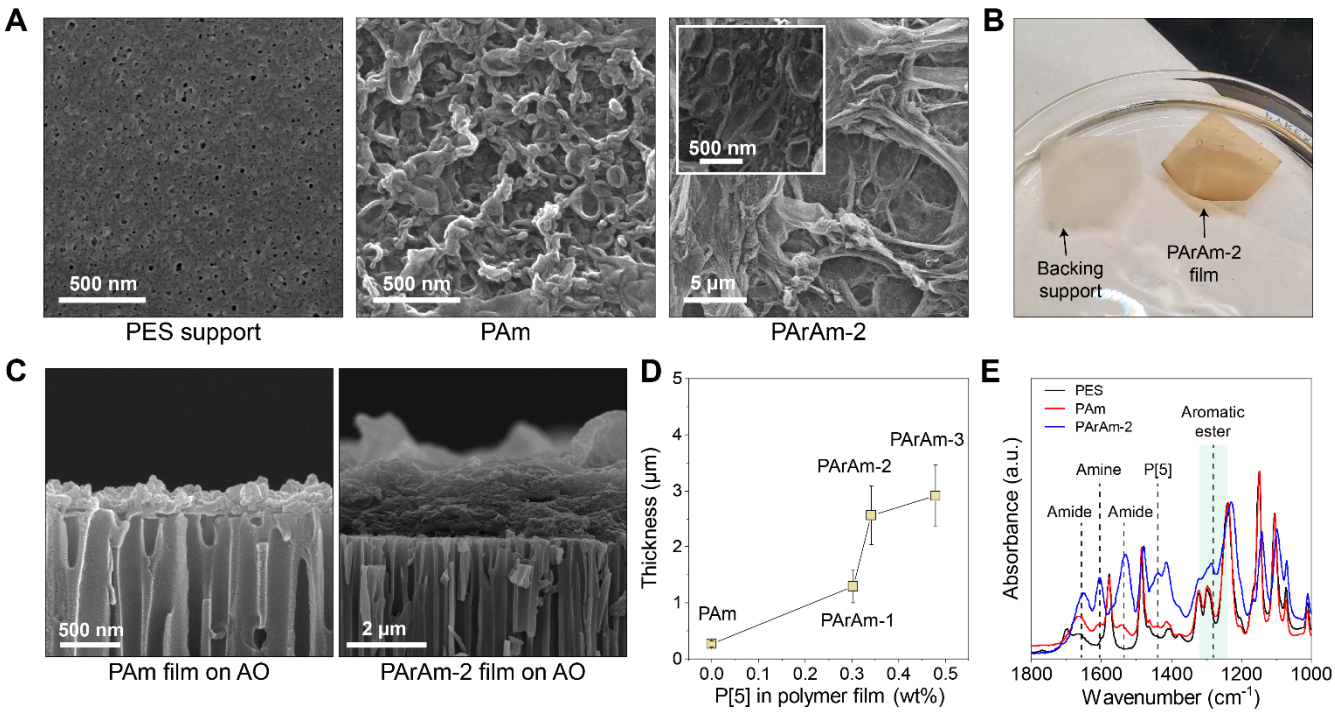

Figure 2. TFC gas separation membranes prepared by IP reactions. (A) Representative SEM images of the polyether sulfone (PES) support, PAm, and PArAm-2 membranes. (B) Photograph of a freestanding PArAm-2 film in dichloromethane (DCM). After the PES polymer is dissolved in DCM, the backing support fabric is separated, and the film is ready to be transferred to another support membrane. (C) Cross sectional SEM images of the PAm and PArAm polymer films after transferring onto an anodized aluminum oxide (AAO) support. (D) Polymer film thickness as a function of P[5] fraction in the polymers. (E) FT-IR spectra of PES, PAm, and PArAm TFC membranes.

Successful polymer film formation by IP was evaluated using scanning electron microscopy (SEM) of both the as-prepared TFC membranes (**Figure 2A** and **Figure S1**) and the free-standing films transferred on aluminum oxide (AO) membranes (**Figure 2B** and **Figure S2 – S6**). PAm membranes present the characteristic film structure of conventional TFC membranes, which is a ridge-and-valley morphology with thicknesses around ~200 nm (**Figure 2C** and **Figure S3**).[11] The PArAm films also have rough surfaces, but the scale of those structures and film thicknesses are much larger than those of PAm membranes, as discussed later (**Figure 2A – D** and **Figure S4 – S6**).

In addition to evaluation of film formation, Fourier-transform infrared (FT-IR) spectroscopy confirmed the integration of P[5]s in the films (**Figure 2E**). For both PAm and PArAm membranes, IR peaks of C=O stretching and N-H bending of the amide bonds are observed at 1630 - 1690 cm^{-1} and 1530 cm^{-1}, respectively. N-H bending of the unreacted MPD amines is also observed at 1610 cm^{-1}. Also, PArAm membranes show aromatic ester peaks at 1310 - 1250 cm^{-1}, indicating covalent bond formation by the

Table 1. Summary of TFC membrane properties.

	XPS			Ratios of the repeating units in polymers			CA[a] (%)	Polymer density (g/cm^3)		FFV normalized to PAm[b]		P[5] in polymer films (w/w %)
	C (%)	N (%)	O (%)	P[5]	MPD	TMC		Ref.	Sim.	Exp.	Sim.	
PA_m	74.5	9.23	16.2		1	1.12	3.85	1.33 – 1.38	1.36	1	1	0
PArAm-1	74.9	6.6	18.5	1	4.96	5.31	11.5		1.45	0.54	0.54	30.3
PArAm-2	75.3	7.6	17.1	1	5.06	3.90	9.83		1.42	0.62	0.63	34.2
PArAm-3	76.0	7.1	16.9	1	3.38	1.88	7.78		1.38	0.89	0.87	47.9

[a]CA (mol %): percentage of free carboxylic acids compared to total available acid chloride groups of TMC in polymer films.
[b]Experimental (Exp.) values are from PALS analysis. Simulation (Sim.) values are analyzed using Zeo++ based on He-void fractions.

reactions between P[5]s and TMCs. The H-C-H in-plane bending at 1450 cm^{-1} is only seen for PA_rA_m membranes, which only exist in the P[5] structures.

The ratios of P[5], MPD, and TMC in the polymer films after IP were further quantified using X-ray photoelectron spectroscopy (XPS) and silver ion (Ag^+) tagging of free carboxylic acids followed by Ag^+ quantification using inductively coupled plasma mass spectroscopy (ICP-MS)[12] (see experimental section for details). As summarized in **Table 1**, the final weight fraction of P[5] was 30.3%, 34.2% and 47.9% for PArAm-1, PArAm-2 and PArAm-3 polymer films, respectively. These incorporation efficiencies are substantially higher than those of conventional porous fillers used for mixed-matrix membrane (MMM) fabrication[13], while maintaining practical stability for gas permeation. The high incorporation efficiency may be attributed to the abundance of crosslinking sites on each monomer structure (**Figure 1A**). Such high fractions of P[5]s suggest that the PArAm polymers should be considered as new polymer networks rather than conventional fillers-in-matrix MMMs. The PArAm matrices also show an interesting relationship between the P[5] fraction and the polymer film thickness. As determined from the cross-sectional SEM analyses, more P[5] incorporation correlates with thicker polymer films (**Figure 2E** and **Figure S3 – S4**). It is hypothesized that, compared to PAm polymers, the PArAm polymer chains lose freedom of rotation during the polycondensation reaction due to the P[5]s, resulting in thicker polymer films (**Figure S7**). Consequently, the PArAm film thicknesses increase up to ~2.5 μm at a P[5] weight fraction of 47.9 % (**Figure 2E**). Compared to traditional IP materials used in water purification, these thicker but still micron-scale thin selective layers may offer better processability of larger scale, defect free membrane fabrication, while maintaining desirable membrane permeance.

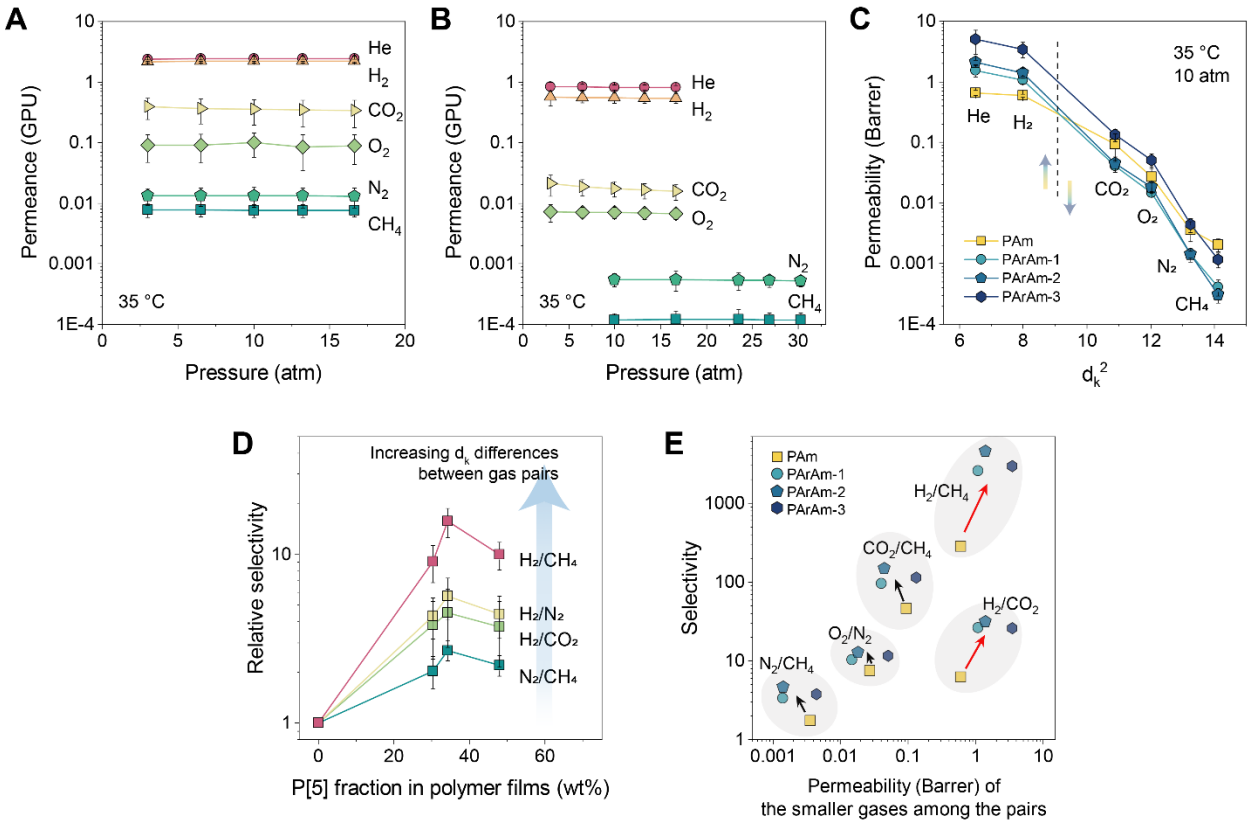

Figure 3. Gas transport properties of PAm and PArAm TFC membranes show enhanced molecular sieving abilities. Gas permeance of (A) PAm and (B) PArAm-2 TFC membranes measured at 35 °C. Error bars are the standard deviation of three independent membrane measurements. (C) Permeability of synthesized membranes as a function of squared kinetic diameters (d_k^2) of the gas molecules 35 °C and 10 atm. (D) Relative selectivity for several representative gas pairs calculated based on gas permeance at 35 °C and 10 atm. Error bars are propagated errors from standard deviations of measurements. (E) Permeability and selectivity plot of both the PAm and the PArAm TFC membranes for several representative gas pairs measured at 35 °C and 10 atm. Arrows indicate the trends of permselectivity changes of the TFC membranes by P[5] incorporation. H_2-coupled gas pairs showed both increased permeability and selectivity (red arrows) due to the exceptionally fast H_2 (and He) permeation in the P[5]-containing membranes compared to the PAm membranes.

Pure-gas permeance of the PAm and PArAm TFC membranes were measured for He, H_2, CO_2, O_2, N_2 and CH_4 (**Figure 3A - B, Figure S8**, and **Table S1 – S2**). Across the pressure range considered, gas permeances are essentially constant, suggesting that no defects were introduced during membrane formation. As shown in **Figure 3C**, gas permeability was estimated based on the resistance-in-series model.[14, 15] (Supporting Information). Gas permeability of PAm and PArAm TFC membranes decreases with increasing kinetic diameter, which shows the molecular sieving ability of the membranes (**Figure 3C**). Also, no geometric restriction was observed from the PES support membranes as confirmed by application of the resistance model (**Table S3**), and the selectivity values of PAm membranes match well with several recent references of commercial or lab-made PAm TFC membranes (**Table S4** and **S5**).[16, 17] Importantly, the addition of P[5]

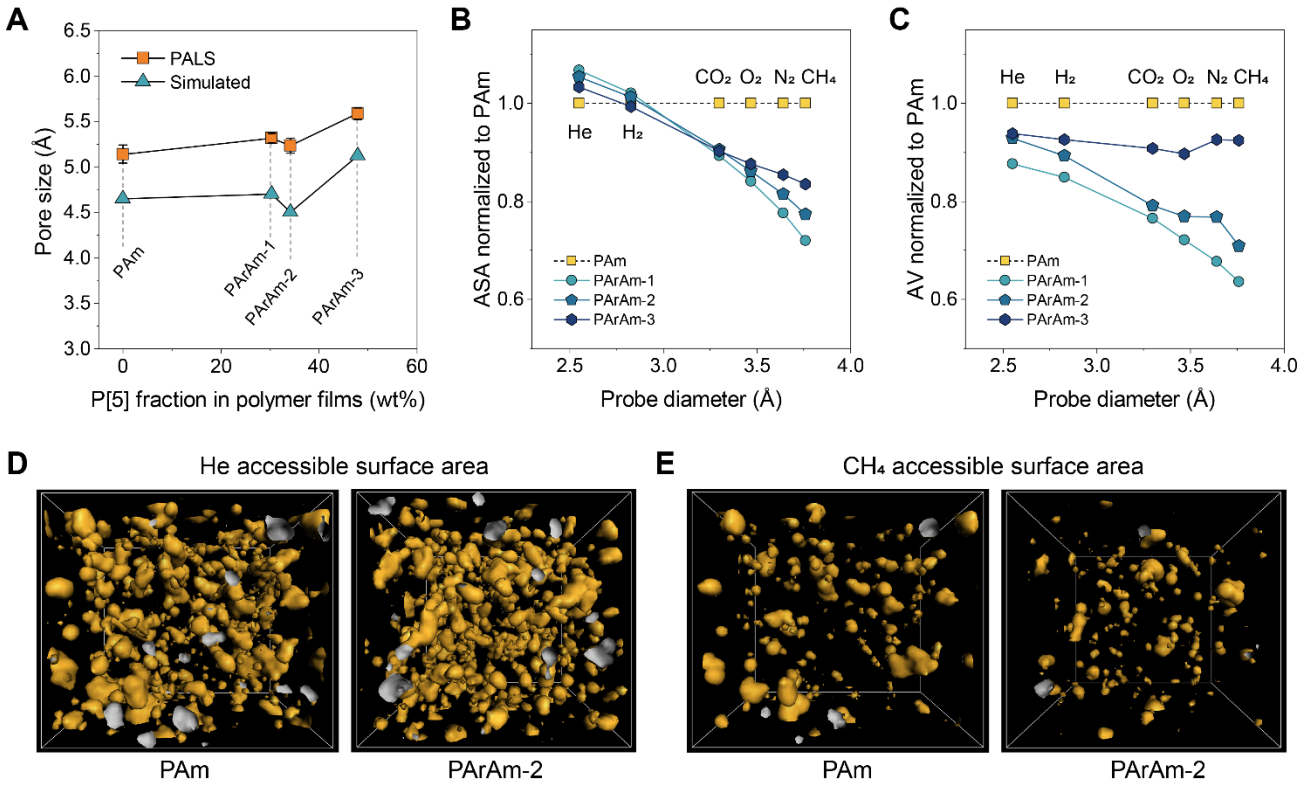

Figure 4. Characterization of PAm and PArAm membranes microstructures using PALS and molecular modeling. (A) Comparison of the average pore size of the isolated polymer films measured by PALS to the largest included spheres of the simulated polymer structures. (B) Accessible surface areas (ASA) and (C) accessible free volumes (AV) of PArAm polymers which are normalized to the PAm membranes' values. Probe diameters used for analysis are the same as the kinetic diameters of the gases. (D and E) Visualized accessible surface areas of the PAm and PArAm-2 polymer models for (D) He and (E) CH_4.

to TFC membranes improves molecular sieving ability. This result is evident in the relative selectivity plot (**Figure 3D**), which is defined as the pure-gas selectivity of the membranes normalized by the PAm membrane selectivity. As P[5] content increases, relative selectivity initially increases. In addition, as the size difference between gas pairs becomes greater, the relative selectivity increases to greater extent, strongly supporting that P[5] incorporation enhances molecular sieving ability in the membranes. Representative pure gas selectivities of PArAm-2 membranes are 32 (H_2/CO_2), 150 (CO_2/CH_4), 4600 (H_2/CH_4), 13 (O_2/N_2), and 4.7 (N_2/CH_4) at 35 °C and 10 atm. The relative selectivity reaches a maximum at 34.2 wt% of P[5] (PArAm-2) and decreases slightly in spite of the higher P[5] content (i.e., 47.9 wt% of PArAm-3). This observation is in accordance with our hypothesis that an optimum ratio of P[5], MPD and TMC would maximize the gas separation properties of PArAm membranes by avoiding forming undesirable voids around P[5] after IP reactions by filling the inter-P[5] spaces with a minimum amount of MPD (**Figure S9**). Due to these reasons, the gas selectivity of PAr TFC membranes prepared without MPD in this study was consistent with Knudsen selectivity.

Permeability and selectivity of several representative gas pairs for both PAm and PArAm membranes are summarized in **Figure 3E**. Interestingly, He and H_2 permeability coefficients of PArAm membranes are noticeably higher than those of PAm membranes and, therefore, the addition of P[5] increases both permeability and selectivity for He- or H_2-paired gases. Such an improvement in permeability/selectivity combinations represents a characteristic structural feature of the PArAm membranes for gas separations.[18]

To obtain molecular scale insights into the microstructures of PArAm membranes, positron annihilation lifetime spectroscopy (PALS) was performed. The PALS data of SW30 Dow Filmtec membranes, which we reported previously using the same experimental conditions, was used as the PAm membrane model.[19] With P[5] incorporation, the average pore size of the membranes became slightly larger from 5.14 Å (PAm) to 5.32 Å (PArAm-1), 5.23 Å (PArAm-2) and 5.59 Å (PArAm-3) (**Figure 4A**) but fractional free volume (FFV) of PArAm membranes is reduced by 54.5%, 62.5% and 89.1% compared to PAm membranes (**Table 1** and **Table S6**). Considering that P[5] possesses specific internal cavities of 4.7Å diameter due to stable carbon-carbon bonds (**Figure 1A**), these significant FFV reductions imply that the surrounding polymer chains became much more densely packed than conventional crosslinked PAm matrices, which favors high levels of molecular sieving.

These microstructures were also identified from our polymer structure modeling simulations. All PAm and PArAm polymer matrices were generated by a 21-step polymerization method[20, 21], reflecting our experimental parameters such as the repeating unit ratios after polymerization, the density of free carboxylic acid in the polymers, and relative FFV differences between the membranes (**Table 1**). The density of PAm (1.3634 g/cm^3) obtained following the 21-step polymerization process is in good agreement with values reported in the literature (1.358 g/cm^3), validating the generated PAm polymer structure model.[20] Due to the absence of experimental PArAm polymer densities, the He-void fractions of the simulated polymer structures were compared to the FFV values obtained from PALS and, for the PArAm polymer models, an additional step of compression was performed followed by equilibration to match these two experimental (PALS-based FFV) and simulation (He-void) parameters (**Table 1**, **Figure S6**, and **Table S7**) (see the experimental section for the details). As a result, the largest included sphere sizes of the generated polymer structures closely relate to the average pore sizes obtained from PALS (**Figure 4A**). Also, accessible surface area was analyzed using different Connolly probe sizes that are the same as the kinetic diameters of the gases (**Figure 4B**). The accessible surface areas of PArAm membranes for CO_2, O_2, N_2, and CH_4 were lower than PAm polymers, as expected from the lower FFV values.

However, the trends were reversed for probe sizes smaller than ~2.8 Å, which corresponds to the size of H_2, and the PArAm membranes show higher accessible surface areas for He and H_2 compared to the PAm membranes despite their lower accessible volumes (**Figure 4C**) or FFV values (**Table 1**). Such lower accessible volumes but higher surface areas are consistent with microstructures of the PArAm membranes having narrow (~2.8 Å) free volume elements that interconnect the P[5] apertures (~4.7 Å) (**Figure 4D** and **4E**) to provide fast permeation paths for He and H_2 as well as significantly enhancing molecular sieving effects for the other gases. This microstructure model is consistent with the permeability (**Figure 3C**) and the accessible surface area (**Figure 4B**) results.

As mentioned above, one of the challenges of using TFC membranes for gas separations has been to avoid defects during IP reactions.[16] In this regard, highly cross-linked PArAm membranes also show promise in terms of making defect-free membranes. Recently, Pinnau and coworkers reported that increasing IP reaction times longer than five minutes could help avoid forming defects during PAm TFC membrane fabrication for gas separations.[17, 22] We also faced the same challenge for PAm membrane fabrication, and we set the IP reaction time to 10 minutes for both initial membrane development and fundamental studies of both PAm and PArAm membranes. However, defect free PArAm TFC membranes could be readily prepared at IP reaction times as low as one minute without compromising the selectivity, while showing increased gas permeance due to the decreased thickness of the selective layers (**Figure S10** and **S11**). In addition, PArAm TFC membranes did not show any obvious structural deformation even under pressures up to 33 atm of CO_2 (**Figure S12**), showing the potential stability of the membranes against plasticization.

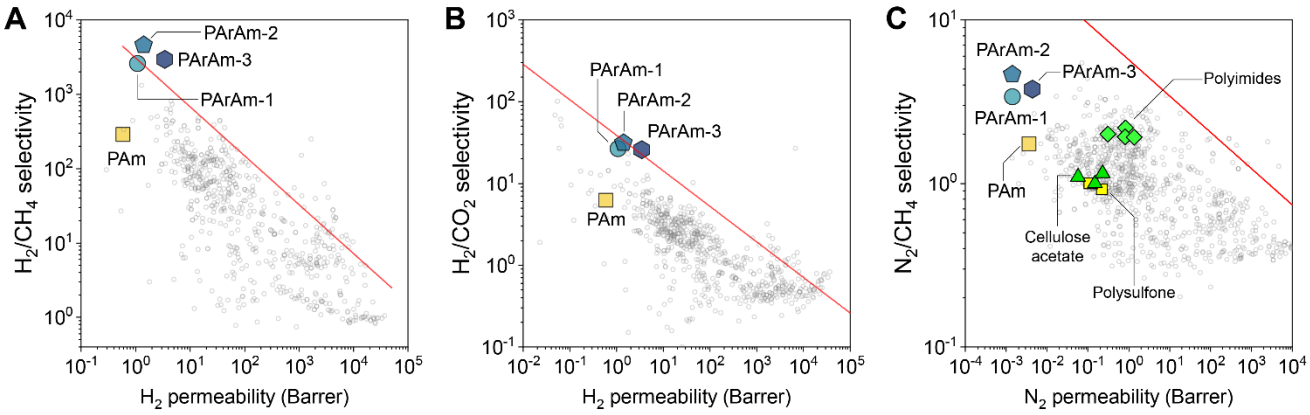

Figure 5. Gas transport property comparison of PAm and PArAm TFC membranes to the Robeson plots for gas pairs of (A) H_2/CH_4, (B) H_2/CO_2 and (C) N_2/CH_4. For the N_2/CH_4 gas pairs, data points of the several glassy polymers (cellulose acetate, polysulfone, and polyimides) that are currently available for large scale applications are plotted together as comparison.

The outstanding molecular sieving ability of the PArAm TFC membranes could be seen when compared to other polymer materials in Robeson plots (**Figure 5**).[23] First, H_2 paired gases' permselectivity is beyond (or near) the upper bound line due to enhanced He and H_2 permeability despite decreased FFV (**Figure 5A** and **B**). For the other gas pairs, although the PArAm membranes are following permeability-selectivity trade-off behavior (**Figure 3E**), their selectivity values outperform those of most polymer materials, suggesting their potential applications for the gases to be separated based on subtle differences in kinetic diameters, such as N_2/CH_4 separations (**Figure 5C**).[4, 24]

3. Conclusion

In summary, P[5]-integrated TFC membranes were prepared by IP. All starting materials are either already being used for large scale membrane production by IP (MPD and TMC) or commercially available (P[5]). Also, IP-based TFC membranes have been the most successful membrane platform in the market, and their capabilities of the large-scale production and physical stability have been thoroughly validated during the past few decades.[6, 25] Therefore, the practical hurdles for scale-up of PArAm membranes at early stage would be meeting the cost requirement for the membrane fabrication, which is often neglected at the stage of lab-scale membrane developments. In this regard, preliminary evaluation of the membrane fabrication cost based on lab-scale chemical synthesis is about ~22 $/m^2 (Supplementary Method, **Table S8** and **Table S9**), which satisfies natural gas process membrane cost limits of 50 $/m^2.[24] The properties of the PArAm TFC membranes, such as the outstanding molecular sieving performance, and the practical stability of the membranes could be important on He or H_2 separations or other important gas separation applications that require enhanced molecular sieving.

4. Experimental Section

P[5] synthesis: All chemicals and solvents were purchased from Sigma Aldrich unless otherwise specified, and they were used without further purification. P[5]s were synthesized following a previously reported method.[26] Detailed procedures are available in Supporting Information.

Membrane fabrication using IP reaction: The TFC membranes were synthesized using the interfacial polymerization technique described elsewhere.[7] In brief, Microdyn Nadir MP-005 poly(ether sulfone) ultrafiltration membranes (PES) were purchased and used as porous support membranes for the TFC membrane fabrication. Before polymerization, the PES membranes were immersed in distilled water and washed for 24 hours, with several water changes to remove membrane humectants and preservatives. To activate the phenolic

reactive groups of pillar[5]arenes to phenoxides, P[5]s and 1.2 × molar excess of NaOH with respect to the number of P[5]s' phenolic groups were dissolved in water. MPD was further dissolved in this solution to prepare aqueous monomer solutions with different monomer concentrations (w/v %). For the PAm membrane preparation, MPD was dissolved in DI water without P[5]s. The final monomer concentrations for each membrane were as follows: PAm (2 w/v% MPD), PArAm-1 (1.5 w/v% P[5] and 0.25 w/v% MPD), PArAm-2 (1.5 w/v% P[5] and 0.5 w/v% MPD), and PArAm-3 (1.5 w/v% P[5] and 0.75 w/v% MPD). The solution was filtered through a 0.2 μm PTFE syringe filter to remove any dust or particulate contaminants. TMC was dissolved in anhydrous *n*-hexane to prepare organic phase monomer solutions with 0.5 w/v%. Before the IP reaction, PES support membranes were immersed in aqueous monomer solutions for five minutes, and then transferred on a glass plate. Excess aqueous solution on the surface of the membranes was removed using a squeegee with a silicone blade. A custom-made PTFE gasket was placed on the surface of the membrane, and the TMC solution was poured into the gasket to the initiate interfacial polymerization. Reaction times for the polymerizations were 10 minutes unless otherwise specified. Reactions were terminated by flushing the TMC solution with fresh hexane. The membranes were placed in an oven at 70 °C for 10 minutes for post-baking and washed in distilled water for 24 hours. The prepared membranes were air-dried for one day, and vacuum-dried at 150 °C for 24 hours to remove any residual solvent (water) in the membranes. Membranes were kept in a desiccator until gas permeation experiments.

Pure gas permeation measurements: Membranes were masked with brass discs (McMaster-Carr, Cat #9011K4) and sealed with epoxy glue before pure gas permeation measurements.[27] The diameter of the brass discs was 47 mm with ~2.8 cm^2 membrane test area (0.75 inch diameter of the central hole). All measurements were performed at 35 °C with varying upstream pressures using a constant-volume and variable-pressure apparatus, which was equipped with a high-pressure filter holder (47 mm, HP Filter Holder, #4504700, MilliporeSigma). A 1000-psig industrial grade pressure transducer (Model STJE, Honeywell) and a 10-torr capacitance manometer (Baratron 626A, MKS) were used to monitor and record the upstream and downstream system pressures, respectively. The downstream pressure was maintained below 10 torr for the duration of the gas permeation experiment. Gas permeance (p) is calculated using the following equation.

$$p\left(10^{-6}\frac{cm^3(STP)}{cm^2\cdot s\cdot cmHg}\right)=\frac{V_d}{p_2ART}\left[\left(\frac{dp_1}{dt}\right)_{ss}-\left(\frac{dp_1}{dt}\right)_{leak}\right]$$

where V_d is the downstream volume, p_2 is the upstream pressure, A is area of the membrane, $\left(\frac{dp_1}{dt}\right)_{ss}$ is steady-state pressure change during the measurement, and $\left(\frac{dp_1}{dt}\right)_{leak}$ is the leak rate. Gas permeability (P) is calculated

using the following equation.

$$P = p \times l$$

where GPU is gas permeance and l is the thickness of polymer film.

Scanning electron microscopy: Top and cross-sectional membrane morphology was investigated using scanning electron microscopy (Quanta 650, FEI) with an accelerating voltage between 5 kV and 20 kV. Samples were coated using an EMS sputter coater with Au:Pd ratio of 60:40, and sputter time was 45 seconds. For the cross-sectional film preparation, PES support layer of TFC membranes were etched with dichloromethane, and free-standing films were transferred onto anodized aluminum oxide (AAO) membranes (Anodisc 0.2 μm pore size, Whatman). AAO-supported films were cryo-fractured using liquid nitrogen and subjected to SEM investigation.

FT-IR: FT-IR spectra of samples were obtained using a Nicolet 6700 spectrometer (Thermo Scientific, Waltham) to probe the chemical structures of the synthesized polymer films. All scanning was performed with 256 scans per sample, with a spectrum resolution of 4 cm^{-1}.

X-ray photoelectron spectroscopy (XPS): XPS analysis was performed to quantify elemental compositions (C, N, O) of polymer films. XPS spectra were obtained using a Kratos AXIs Ultra DLD spectrometer with a monochromatic Al-Kα X-ray source (hv = 1486.5 eV) with a spot size of 400 μm. All binding energies were adjusted to the adventitious C1s signal at 284.8 eV. The peaks were analyzed using CasaXPS software.

Quantifying free carboxylic acid in polymers using inductively coupled plasma mass spectroscopy (ICP-MS): Carboxylic acid density in the selective layers of PArAm membranes after IP reactions was quantified using the method first proposed by Elimelech and coworkers[12], based on tagging carboxylic acid groups with Ag^+ proposed by Coronell *et al*.[28] This method uses Ag^+ ions as molecular probes to detect free carboxylic acids by ion association. In brief, PArAm polymer films were isolated by immersing the membranes in DCM to dissolve the PES support layers. Free standing polymer films were then washed with an excess volume of methanol and vacuum dried at 150 °C for 24 h to completely remove any residual solvent. Dried films were weighed. Polymer films were immersed in the binding solution (40 μM $AgNO_3$ in distilled water at pH 10.5) for 10 minutes and transferred to fresh binding solution and incubated for another hour on an orbital shaker. After this binding step, films were transferred to the rinsing solution (1 μM $AgNO_3$ in distilled water at pH 10.5) to rinse off any unbound Ag^+ ions in and around the films. The rinsing solution was replaced four times with new solution every 7 minutes. Lastly, films were transferred

to 20 mL of elution solution (2% nitric acid, trace metal grade chemical solution) for two hours. After the elution step, films were removed, and the elution buffer was subjected to ICP-MS to measure the concentration of Ag^+ ions in the solution. Since carboxylic acid reactive groups associate with Ag^+ ions at a molar ratio of 1:1, the carboxylic acid density per unit mass of polymer was calculated from the amount of Ag^+ ions eluted from a given polymer weight.

Calculation of the ratio of monomer units in polymer films after IP reaction: Three mass balance equations of C, O, and N were used to calculate the ratio of various monomers incorporated in the films, based on the quantitative C, O, and N ratios obtained from XPS analysis. For PAm membranes, there are three unknown variables after IP reactions, which are the ratio of MPD over TMC and the density of free carboxylic acid. Therefore, the equations could be solved using the XPS results. More datils of this calculation is shown in **Figure S14**. For the PArAm membranes, there are four unknown variables which are the ratios of P[5], MPD and TMC, and the density of free carboxylic acids. Therefore, the density of free carboxylic acid was first analyzed separately using the ICP-MS experiments, and then the equations were solved to find the repeating unit ratios of P[5], MPD, and TMC monomers.

Positron annihilation lifetime spectroscopy (PALS): PALS measurements were performed using an EG&G Ortec fast-fast coincident system. PArAm membrane films were isolated from the synthesized membranes by immersing in DCM. The films were thoroughly washed with excess amounts of DCM and then methanol, and vacuum dried at 150 °C for 24 hours. A positron source (approx. 1.5 MBq of Na-22 sealed in Mylar) was placed in the center of a 3 mm thick bundle of membrane films. The samples were run under vacuum (1 x 10^{-6} torr), and data was collected for 5 files each with a minimum of 4.5 x 10^6 integrated counts per file. The spectra were analyzed using LT_v9 software[29] and fit to three lifetime components. The first component was fixed to 0.125 ns due to para-positronium annihilation (bound state of the positron with an electron of opposite spin). The second component (approx. 0.4 ns) was due to positrons annihilating with free electrons within the samples. The third component was due to ortho-positronium (o-P) annihilation (bound state of positron and electron of the same spin). This o-Ps lifetime is related to the free-volume within the samples.[30] The size of the free volume element, *r*, was determined via a semi-empirical Tao-Eldrup relationship.[31, 32]

$$\tau_3 = \frac{1}{2}\left(1 - \frac{r}{r+\Delta r} + \frac{1}{2\pi} sin\left[\frac{2\pi r}{r+\Delta r}\right]\right)^{-1}$$

where Δr is an empirical constant related to the electron layer thickness and calculated to be 1.66Å. The

Fractional Free Volume for PALS (FFV_{PALS}) was calculated using the relationship

$$FFV_{PALS} = c \times V \times I$$

Here, V is the average spherical pore volume calculated from the PALS radius, $^{4\pi}/_{3}\, r^3$, I is the PALS intensity which is representative of the average number of pores in the sample, and c is a constant empirically determined to be 0.0018 nm^{-3} for several polymers.[33]

Polymer structure simulations and analysis: The initial monomer units were minimized using B3LYP level of theory of DFT formalism along with 6-31G(d,p) basis set.[34-37] Further the partial charges were calculated using HF/6-31G* level of theory in the gas phase followed by RESP. using Gaussian03 (**Figure S7** and **S8,** and **Table S10** and **S11**).[34, 38] The bonded and non-bonded interactions of all the constituents were modelled using GAFF.[39] To form cross-linked morphology from the monomers, Polymatic was used.[40] This process is divided into the following steps. First, the monomers are packed randomly in a box at a low density of 0.2 g/cm^3. The number of different MPD, TMC and P[5] monomers are in the ratio obtained from experiment. Next, a series of short NVT simulations at 600K are done allowing the monomers to rearrange themselves rapidly. When the terminal carbon atom of TMC comes within 3 Å of either a terminal nitrogen atom of MPD or a terminal oxygen atom of P[5], a new bond is created between them. The terminal bonding atoms are given an addition charge of ± 0.3e to facilitate their rate of approach. This excess charge is removed as soon as a pair of terminal atoms undergo bond formation. The addition of this fictitious charge has been shown to increase the bonding rate without altering the structure of the generated morphology.[40] This cycle of NVT equilibration and bond formation is continued until all the monomers have linked with each other. Any unbonded, freely dangling monomer unit is removed completely. The terminal ends of the final structure are capped using the appropriate capping groups (H for amide group of MPD, OH for carbonyl group TMC and H for phenol group of P[5]). The crosslinked structure thus obtained using Polymatic has a density ~ 0.3 g/cm^3. This crosslinked structure is next subjected to a 21-step polymerization protocol[19] using LAMMPS.[41]

Here, the system undergoes rapid compression and decompression cycles of extremely high pressures. The 21-step polymerization protocol comprises first an NVT simulation at 1000 K for 10000 steps, an NVT simulation at 300 K for 50000 steps, and an NPT simulation at 300 K with pressure P for 50000 steps. These three steps are repeated seven times, where the pressure P is different for each NPT simulation as shown in **Figure S13**. The maximum pressure used in this protocol is 5×10^4 atm. A timestep of 2 fs is

used. SHAKE algorithm[42] was used to constrain the bonds involving hydrogen atoms. The temperature and pressures were maintained using Nose-Hoover thermostat and barostat[43, 44] with both coupling constants being 200 fs . He-void fractions of the 21-step morphology was computed using RASPA.[45]

In the absence of experimental density data for PArAm polymers, the He-void fraction of these structures were compared with the experimental FFV results. The He-Void fraction from the 21-step polymerization protocol deviates from experimentally observed FFVs. This discrepancy may arise due to multiple reasons: choice of forcefield for the P[5]s, mechanism of crosslinking of the monomers in these membranes or even the rate of compression and decompression done during the 21-step process. The extent of this compression or decompression is not known a priori, thus requiring a series of simulations to be performed until the structures with desired FFVs as found in PALS experiments are obtained (**Table 1**). Therefore, for PArAm polymers, the structures obtained using the 21-step polymerization are subjected to compression using NVT ensemble by reducing the simulation box volume in steps. This compression is continued until their He-void fraction (normalized with respect to PAm) show the same trend as obtained from PALS experiments. We find that these densities are higher compared to densities obtained after 21-step polymerization process. The high densities suggest tight packing of monomers around the P[5] rings as discussed earlier.

Supporting Information

P[5] synthesis; Cost evaluation for membrane fabrication; Resistance model calculation; SEM analyses; Gas permeance data; PALS data; Polymer structure modeling data

Acknowledgements

The authors acknowledge financial support from the National Science Foundation (NSF) CAREER grant (CBET-1552571) to MK for this work. Additional support was provided by NSF grant CBET- 1804836.

Conflict of interest

The authors declare no conflict of interest.

Data availability statement

The datasets that support the finding of this study are available in Zenodo repository with identifier (http://doi.org/10.5281/zenodo.6784653).

Present Address

[#]W.S.: Department of Chemistry, University of California, Berkeley, CA 94720, USA

References

1. Sholl, D. S.; Lively, R. P., Seven chemical separations to change the world. *Nature* **2016,** *532* (7600), 435-437.

2. Lai, H. W. H.; Benedetti, F. M.; Ahn, J. M.; Robinson, A. M.; Wang, Y.; Pinnau, I.; Smith, Z. P.; Xia, Y., Hydrocarbon ladder polymers with ultrahigh permselectivity for membrane gas separations. *Science* **2022,** *375* (6587), 1390-1392.

3. Koros, W. J.; Zhang, C., Materials for next-generation molecularly selective synthetic membranes. *Nature Materials* **2017,** *16* (3), 289-297.

4. Baker, R. W.; Low, B. T., Gas Separation Membrane Materials: A Perspective. *Macromolecules* **2014,** *47* (20), 6999-7013.

5. Baker, R. W., Future Directions of Membrane Gas Separation Technology. *Industrial & Engineering Chemistry Research* **2002,** *41* (6), 1393-1411.

6. Seah, M. Q.; Lau, W. J.; Goh, P. S.; Tseng, H.-H.; Wahab, R. A.; Ismail, A. F., Progress of Interfacial Polymerization Techniques for Polyamide Thin Film (Nano)Composite Membrane Fabrication: A Comprehensive Review. *Polymers* **2020,** *12* (12), 2817.

7. Xie, W.; Geise, G. M.; Freeman, B. D.; Lee, H.-S.; Byun, G.; McGrath, J. E., Polyamide interfacial composite membranes prepared from m-phenylene diamine, trimesoyl chloride and a new disulfonated diamine. *Journal of Membrane Science* **2012,** *403-404*, 152-161.

8. Villalobos, L. F.; Huang, T.; Peinemann, K.-V., Cyclodextrin Films with Fast Solvent Transport and Shape-Selective Permeability. *Advanced Materials* **2017,** *29* (26), 1606641.

9. Zhao, Q.; Liu, Y., Macrocycle crosslinked mesoporous polymers for ultrafast separation of organic dyes. *Chemical Communications* **2018,** *54* (53), 7362-7365.

10. Lee, J.; Zhou, F.; Baek, K.; Kim, W.; Su, H.; Kim, K.; Wang, R.; Bae, T.-H., Use of rigid cucurbit[6]uril mediating selective water transport as a potential remedy to improve the permselectivity and durability of reverse osmosis membranes. *Journal of Membrane Science* **2021,** *623*, 119017.

11. Culp, T. E.; Khara, B.; Brickey, K. P.; Geitner, M.; Zimudzi, T. J.; Wilbur, J. D.; Jons, S. D.; Roy, A.; Paul, M.; Ganapathysubramanian, B.; Zydney, A. L.; Kumar, M.; Gomez, E. D., Nanoscale control of internal inhomogeneity enhances water transport in desalination membranes. *Science* **2021,** *371* (6524), 72-75.

12. Chen, D.; Werber, J. R.; Zhao, X.; Elimelech, M., A facile method to quantify the carboxyl group areal density in the active layer of polyamide thin-film composite membranes. *Journal of Membrane*

Science **2017,** *534*, 100-108.

13. Qian, Q.; Asinger, P. A.; Lee, M. J.; Han, G.; Mizrahi Rodriguez, K.; Lin, S.; Benedetti, F. M.; Wu, A. X.; Chi, W. S.; Smith, Z. P., MOF-Based Membranes for Gas Separations. *Chemical Reviews* **2020,** *120* (16), 8161-8266.

14. Rowe, B. W.; Freeman, B. D.; Paul, D. R., Physical aging of ultrathin glassy polymer films tracked by gas permeability. *Polymer* **2009,** *50* (23), 5565-5575.

15. Henis, J. M. S.; Tripodi, M. K., Composite hollow fiber membranes for gas separation: the resistance model approach. *Journal of Membrane Science* **1981,** *8* (3), 233-246.

16. Park, J.; Yoon, H. W.; Paul, D. R.; Freeman, B. D., Gas transport properties of PDMS-coated reverse osmosis membranes. *Journal of Membrane Science* **2020,** *604*, 118009.

17. Ali, Z.; Pacheco, F.; Litwiller, E.; Wang, Y.; Han, Y.; Pinnau, I., Ultra-selective defect-free interfacially polymerized molecular sieve thin-film composite membranes for H2 purification. *Journal of Materials Chemistry A* **2018,** *6* (1), 30-35.

18. Freeman, B. D., Basis of Permeability/Selectivity Tradeoff Relations in Polymeric Gas Separation Membranes. *Macromolecules* **1999,** *32* (2), 375-380.

19. Lee, J.; Doherty, C. M.; Hill, A. J.; Kentish, S. E., Water vapor sorption and free volume in the aromatic polyamide layer of reverse osmosis membranes. *Journal of Membrane Science* **2013,** *425-426*, 217-226.

20. Liyana-Arachchi, T. P.; Sturnfield, J. F.; Colina, C. M., Ultrathin Molecular-Layer-by-Layer Polyamide Membranes: Insights from Atomistic Molecular Simulations. *The Journal of Physical Chemistry B* **2016,** *120* (35), 9484-9494.

21. Larsen, G. S.; Lin, P.; Hart, K. E.; Colina, C. M., Molecular Simulations of PIM-1-like Polymers of Intrinsic Microporosity. *Macromolecules* **2011,** *44* (17), 6944-6951.

22. Ali, Z.; Wang, Y.; Ogieglo, W.; Pacheco, F.; Vovusha, H.; Han, Y.; Pinnau, I., Gas separation and water desalination performance of defect-free interfacially polymerized para-linked polyamide thin-film composite membranes. *Journal of Membrane Science* **2021,** *618*, 118572.

23. Robeson, L. M., The upper bound revisited. *Journal of Membrane Science* **2008,** *320* (1), 390-400.

24. Lokhandwala, K. A.; Pinnau, I.; He, Z.; Amo, K. D.; DaCosta, A. R.; Wijmans, J. G.; Baker, R. W., Membrane separation of nitrogen from natural gas: A case study from membrane synthesis to commercial deployment. *Journal of Membrane Science* **2010,** *346* (2), 270-279.

25. Lu, X.; Elimelech, M., Fabrication of desalination membranes by interfacial polymerization:

history, current efforts, and future directions. *Chemical Society Reviews* **2021,** *50* (11), 6290-6307.

26. Ogoshi, T.; Kanai, S.; Fujinami, S.; Yamagishi, T.-a.; Nakamoto, Y., para-Bridged Symmetrical Pillar[5]arenes: Their Lewis Acid Catalyzed Synthesis and Host–Guest Property. *Journal of the American Chemical Society* **2008,** *130* (15), 5022-5023.

27. Czichos, H.; Saito, T.; Smith, L. E., *Springer Handbook of Materials Measurement Methods*. Springer Berlin Heidelberg: 2007.

28. Coronell, O.; Mariñas, B. J.; Zhang, X.; Cahill, D. G., Quantification of Functional Groups and Modeling of Their Ionization Behavior in the Active Layer of FT30 Reverse Osmosis Membrane. *Environmental Science & Technology* **2008,** *42* (14), 5260-5266.

29. Kansy, J., Microcomputer program for analysis of positron annihilation lifetime spectra. *Nuclear Instruments and Methods in Physics Research Section A: Accelerators, Spectrometers, Detectors and Associated Equipment* **1996,** *374* (2), 235-244.

30. Jean, Y. C.; Mallon, P. E.; Schrader, D. M., *Principles and Applications of Positron and Positronium Chemistry*; World Scientific: River Edge, NJ, 2003.

31. Tao, S. J., Positronium Annihilation in Molecular Substances. *The Journal of Chemical Physics* **1972,** *56* (11), 5499-5510.

32. Eldrup, M.; Lightbody, D.; Sherwood, J. N., The temperature dependence of positron lifetimes in solid pivalic acid. *Chemical Physics* **1981,** *63* (1), 51-58.

33. Ju, H.; Sagle, A. C.; Freeman, B. D.; Mardel, J. I.; Hill, A. J., Characterization of sodium chloride and water transport in crosslinked poly(ethylene oxide) hydrogels. *Journal of Membrane Science* **2010,** *358* (1), 131-141.

34. Cornell, W. D.; Cieplak, P.; Bayly, C. I.; Gould, I. R.; Merz, K. M.; Ferguson, D. M.; Spellmeyer, D. C.; Fox, T.; Caldwell, J. W.; Kollman, P. A., A Second Generation Force Field for the Simulation of Proteins, Nucleic Acids, and Organic Molecules. *Journal of the American Chemical Society* **1995,** *117* (19), 5179-5197.

35. Becke, A. D., Density-functional exchange-energy approximation with correct asymptotic behavior. *Physical Review A* **1988,** *38* (6), 3098-3100.

36. Lee, C.; Yang, W.; Parr, R. G., Development of the Colle-Salvetti correlation-energy formula into a functional of the electron density. *Physical Review B* **1988,** *37* (2), 785-789.

37. Xu, X.; Goddard, W. A., The X3LYP extended density functional for accurate descriptions of nonbond interactions, spin states, and thermochemical properties. *Proceedings of the National Academy*

of Sciences of the United States of America **2004,** *101* (9), 2673-2677.

38. Bayly, C. I.; Cieplak, P.; Cornell, W.; Kollman, P. A., A well-behaved electrostatic potential based method using charge restraints for deriving atomic charges: the RESP model. *The Journal of Physical Chemistry* **1993,** *97* (40), 10269-10280.

39. Wang, J.; Wolf, R. M.; Caldwell, J. W.; Kollman, P. A.; Case, D. A., Development and testing of a general amber force field. *Journal of Computational Chemistry* **2004,** *25* (9), 1157-1174.

40. Abbott, L. J.; Hart, K. E.; Colina, C. M., Polymatic: a generalized simulated polymerization algorithm for amorphous polymers. *Theoretical Chemistry Accounts* **2013,** *132* (3), 1334.

41. Plimpton, S.; Crozier, P.; Thompson, A., LAMMPS-large-scale atomic/molecular massively parallel simulator. *Sandia National Laboratories* **2007,** *18*, 43.

42. Ryckaert, J.-P.; Ciccotti, G.; Berendsen, H. J. C., Numerical integration of the cartesian equations of motion of a system with constraints: molecular dynamics of n-alkanes. *Journal of Computational Physics* **1977,** *23* (3), 327-341.

43. Nosé, S., A unified formulation of the constant temperature molecular dynamics methods. *The Journal of Chemical Physics* **1984,** *81* (1), 511-519.

44. Martyna, G. J.; Klein, M. L.; Tuckerman, M., Nosé–Hoover chains: The canonical ensemble via continuous dynamics. *The Journal of Chemical Physics* **1992,** *97* (4), 2635-2643.

45. Dubbeldam, D.; Calero, S.; Ellis, D. E.; Snurr, R. Q., RASPA: molecular simulation software for adsorption and diffusion in flexible nanoporous materials. *Molecular Simulation* **2016,** *42* (2), 81-101.

Table of Contents